52. Ihara, K., Amemiya, T., Miyashita, Y. & Mukohata, Y. (1994). Met-145 is a key residue in the dark adaptation of bacteriorhodopsin homologs. *Biophys. J.* **67**, 1187–1191.
53. Luecke, H., Richter, H. T. & Lanyi, J. K. (1998). Proton transfer pathways in bacteriorhodopsin at 2.3 angstrom resolution. *Science*, **280**, 1934–1937.
54. Phatak, P., Ghosh, N., Yu, H., Cui, Q. & Elstner, M. (2008). Amino acids with an intermolecular proton bond as proton storage site in bacteriorhodopsin. *Proc. Natl Acad. Sci. USA*, **105**, 19672–19677.
55. Zimányi, L., Varo, G., Chang, M., Ni, B., Needleman, R. & Lanyi, J. K. (1992). Pathways of proton release in the bacteriorhodopsin photocycle. *Biochemistry*, **31**, 8535–8543.
56. Balashov, S. P., Imasheva, E. S., Govindjee, R. & Ebrey, T. G. (1996). Titration of aspartate-85 in bacteriorhodopsin: what it says about chromophore isomerization and proton release. *Biophys. J.* **70**, 473–481.
57. Luecke, H., Schobert, B., Richter, H. T., Cartailler, J. P. & Lanyi, J. K. (1999). Structural changes in bacteriorhodopsin during ion transport at 2 Å resolution. *Science*, **286**, 255–260.
58. Shi, L., Yoon, S. R., Bezerra, A. G., Jr, Jung, K. H. & Brown, L. S. (2006). Cytoplasmic shuttling of protons in *Anabaena* sensory rhodopsin: implications for signaling mechanism. *J. Mol. Biol.* **358**, 686–700.
59. Kawanabe, A., Furutani, Y., Jung, K. H. & Kandori, H. (2009). Engineering an inward proton transport from a bacterial sensor rhodopsin. *J. Am. Chem. Soc.* **131**, 16439–16444.
60. Kawanabe, A., Furutani, Y., Jung, K. H. & Kandori, H. (2010). An inward proton transport using *Anabaena* sensory rhodopsin. *J. Microbiol.* **49**, 1–6.
61. Schneider, S. U., Leible, M. B. & Yang, X.-P. (1989). Strong homology between the small subunit of ribulose-1,5-biphosphatecarboxylase/oxygenase of two species of *Acetabularia* and the occurrence of unusual codon usage. *Mol. Gen. Genet.* **218**, 445–452.
62. Seki, A., Miyauchi, S., Hayashi, S., Kikukawa, T., Kubo, M., Demura, M. *et al.* (2007). Heterologous expression of *pharaonis* halorhodopsin in *Xenopus laevis* oocytes and electrophysiological characterization of its light-driven Cl^- pump activity. *Biophys. J.* **92**, 2559–2569.
63. He, F., Saito, K., Kobayashi, N., Harada, T., Watanabe, S., Kigawa, T. *et al.* (2009). Structural and functional characterization of the NHR1 domain of the *Drosophila* neuralized E3 ligase in the notch signaling pathway. *J. Mol. Biol.* **393**, 478–495.
64. Gill, S. C. & Hippel, P. H. (1989). Calculation of protein extinction coefficients from amino acid sequence data. *Anal. Biochem.* **182**, 319–326.
65. Sato, M., Kubo, M., Aizawa, T., Kamo, N., Kikukawa, T., Nitta, K. & Demura, M. (2005). Role of putative anion-binding sites in cytoplasmic and extracellular channels of *Natronomonas pharaonis* halorhodopsin. *Biochemistry*, **44**, 4775–4784.
66. Landau, E. M. & Rosenbush, J. P. (1996). Lipidic cubic phases: a novel concept for the crystallization of membrane proteins. *Proc. Natl Acad. Sci. USA*, **93**, 14532–14535.
67. Hato, M., Yamashita, I., Kato, T. & Abe, Y. (2004). Aqueous phase behavior of a 1-*O*-phytanyl-β-D-xyloside/water system. Glycolipid-based bicontinuous cubic phases of crystallographic space groups *Pn3m* and *Ia3d*. *Langmuir*, **20**, 11366–11373.
68. Hato, M., Yamashita, J. & Shiono, M. (2009). Aqueous phase behavior of lipids with isoprenoid type hydrophobic chains. *J. Phys. Chem. B*, **113**, 10196–10209.
69. Otwinowski, Z. & Minor, W. (1997). Processing of X-ray diffraction data collected in oscillation mode. *Methods Enzymol.* **276**, 307–326.
70. Collaborative Computational Project, Number 4. (1994). The CCP4 suite: programs for protein crystallography. *Acta Crystallogr., Sect. D: Biol. Crystallogr.* **50**, 760–763.
71. Brunger, A. T., Adams, P. D., Clore, G. M., DeLano, W. L., Gros, P., Grosse-Kunstleve, R. W. *et al.* (1998). Crystallography & NMR system: a new software suite for macromolecular structure determination. *Acta Crystallogr., Sect. D: Biol. Crystallogr.* **54**, 905–921.
72. Emsley, P., Lohkamp, B., Scott, W. G. & Cowtan, K. (2010). Features and development of Coot. *Acta Crystallogr., Sect. D: Biol. Crystallogr.* **66**, 486–501.

BIOCHEMISTRY
including biophysical chemistry & molecular biology

Article

pubs.acs.org/biochemistry

Photochemistry of *Acetabularia* Rhodopsin II from a Marine Plant, *Acetabularia acetabulum*

Takashi Kikukawa,[†] Kazumi Shimono,[‡,§] Jun Tamogami,[†,§] Seiji Miyauchi,[§,∥] So Young Kim,[⊥] Tomomi Kimura-Someya,[‡] Mikako Shirouzu,[‡] Kwang-Hwan Jung,[⊥] Shigeyuki Yokoyama,[*,‡,#] and Naoki Kamo[*,§]

[†]Faculty of Life Science, Hokkaido University, Sapporo 060-0810, Japan

[‡]RIKEN Systems and Structural Biology Center, Yokohama 230-0045, Japan

[§]College of Pharmaceutical Sciences, Matsuyama University, Matsuyama, Ehime 790-8578, Japan

[∥]Graduate School of Pharmaceutical Sciences, Toho University, Funabashi, Chiba 274-8510, Japan

[⊥]Department of Life Science and Institute of Biological Interfaces, Sogang University, Seoul 121-742, Korea

[#]Department of Biophysics and Biochemistry, Graduate School of Science, University of Tokyo, Tokyo 113-0033, Japan

ABSTRACT: *Acetabularia* rhodopsins are the first microbial rhodopsins discovered in a marine plant organism, *Acetabularia acetabulum*. Previously, we expressed *Acetabularia* rhodopsin II (ARII) by a cell-free system from one of two opsin genes in *A. acetabulum* cDNA and showed that ARII is a light-driven proton pump [Wada, T., et al. (2011) *J. Mol. Biol. 411*, 986−998]. In this study, the photochemistry of ARII was examined using the flash-photolysis technique, and data were analyzed using a sequential irreversible model. Five photochemically defined intermediates (P_i) were sufficient to simulate the data. Noticeably, both P_3 and P_4 contain an equilibrium mixture of M, N, and O. Using a transparent indium tin oxide electrode, the photoinduced proton transfer was measured over a wide pH range. Analysis of the pH-dependent proton transfer allowed estimation of the pK_a values of some amino acid residues. The estimated values were 2.6, 5.9 (or 6.3), 8.4, 9.3, 10.5, and 11.3. These values were assigned as the pK_a of Asp81 (Asp85^{BR}) in the dark, Asp92 (Asp96^{BR}) at N, Glu199 (Glu204^{BR}) at M, Glu199 in the dark, an undetermined proton-releasing residue at the release, and the pH to start denaturation, respectively. Following this analysis, the proton transfer of ARII is discussed.

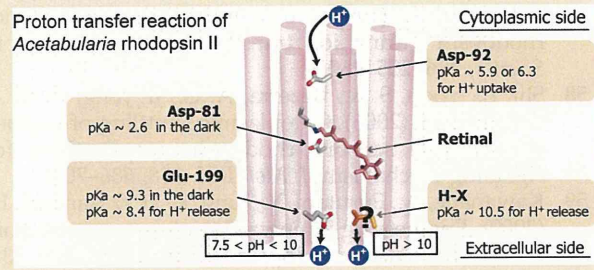

Rhodopsin is a membrane protein in which retinal as a chromophore binds to the lysine residue of the opsin (apoprotein) via a Schiff base. There are two types of rhodopsins.[1] One is type 2 rhodopsin, which is found in the eyes of animals, and the other is type 1 rhodopsin, which is now also called microbial rhodopsin. Originally, type 1 rhodopsin was found in haloarchaea in the early 1970s in the form of a light-driven proton pump, bacteriorhodopsin (BR).[2,3] Later, homologues with different functions were discovered, including halorhodopsin (HR),[4−6] sensory rhodopsin I (SRI),[7−9] and sensory rhodopsin II (SRII, also called phoborhodopsin).[10−14] These proteins have similar structural folds composed of seven helices and retinal binding to the conserved lysine residue of the last helix, whereas the function is different when essential amino acid residues are optimized. BR and HR are ion pumps, and SRI and SRII are photoreceptors. Type 1 rhodopsins have linear cyclic photochemical reactions called photocycles. The illumination of the pigment protein leads to the excited state, which is relaxed thermally to the original pigment via various photochemical intermediates. The best-studied rhodopsin is BR. BR at the ground state and intermediates K−O have been researched with various spectroscopic methods and X-ray crystallography.[2,3] The photocycle comprises stepwise reactions of the thermal reisomerization of the photoisomerized 13-*cis*-retinal to the initial all-*trans*-retinal, and the proton is transferred toward the higher-pK_a residue accompanied by pK_a changes during the photocycle. Type 1 rhodopsins have been found not only in archaea but also in eubacteria, fungi, and algae, and thus, type 1 rhodopsins are classified as microorganisms belonging to all three biological domains.[1] Many type 1 rhodopsins function as either ion pumps with fast photocycles or photoreceptors with slow photocycles. In addition, a new type, a photogated ion channel, was added recently to the family of type 1 rhodopsins on the basis of a study of *Chlamydomonas*.[15−17] Thus, the world of the type 1 rhodopsin (microbial rhodopsin) continues to expand.[1]

As early as 1968, Schilde[18] reported a fast light-induced transmembrane voltage change from a giant unicellular marine alga, *Acetabularia acetabulum*, and on the basis of these results suggested that rhodopsin acts as a photoreceptor. In 2004,

Received: June 28, 2011
Revised: September 5, 2011
Published: September 12, 2011

dx.doi.org/10.1021/bi2009932|*Biochemistry* 2011, 50, 8888−8898

Mandoli and co-workers[19] reported a possible opsin-encoding gene from juvenile *Acetabularia*. Later, Hegemann and co-workers[20] cloned a full-length opsin cDNA from *Acetabularia* and succeeded in expressing the opsin in the *Xenopus* oocyte. This rhodopsin is named *Acetabularia* rhodopsin (AR). They observed a photoinduced current through the oocyte membrane in the presence of various ion species and concluded that AR is a light-driven proton pump. Detailed analysis of the electric current across the oocyte was conducted using the analogy of enzymatic analysis.[21] However, the photochemistry has not yet been examined because sufficient amounts of the AR protein were not available for detailed examination.

We intended to elucidate the photochemistry and structure of AR. For this purpose, the establishment of a large-scale expression system is necessary. Some of us (K.-H.J. and S.Y.K.) recloned an opsin gene from juvenile *Acetabularia* and obtained two possible clones [named ARI and ARII (GenBank accession numbers HM070407 and HM070408, respectively)]. These clones were somewhat different from that of Tsunoda et al.[20] Next, an attempt was made to express these clones in the *Escherichia coli* cell membrane, but the amounts expressed were so small that only the qualitative properties of photochemistry were obtained.[22] On the other hand, Shimono et al. devised a unique cell-free membrane protein synthesis system.[23] The expression of membrane proteins by the cell-free system is usually hindered by the problem that the synthesized peptide is not soluble, which gives rise to denaturation. To circumvent this problem, they conducted the synthesis in the presence of both lipids and detergent, and the detergent was gradually removed during the course of synthesis so that the protein was incorporated into lipid phases. Sufficient amounts of ARII were successfully obtained using this expression system. In a previous paper,[24] it was reported that (1) ARII is a light-driven proton pump, which is the same as AR, (2) the λ_{max} was 533.5 nm, (3) the chromophore was all-*trans*-retinal and no light−dark adaptation occurred, (4) proton uptake occurred first followed by release at 400 mM NaCl and pH 7.0, and (5) the X-ray structure was presented at 3.2 Å resolution. In this work, the photocycle and the proton transfer of ARII are examined over a wide pH range. From the proton transfer measurements using a transparent ITO (indium tin oxide) electrode, the pK_a values of several amino acid residues are estimated. Finally, a possible proton transport mechanism in ARII is discussed.

MATERIALS AND METHODS

Cell-Free Expression and Purification. The cDNA encoding ARII truncated at position 229 was attached by overlap polymerase chain reaction (PCR) to the T7 promoter sequence, the ribosome-binding site, the N11 tag, the cleavage site for tobacco etch virus (TEV) protease, and the T7 terminator sequence.[25] The N11 tag was a modified version of the NHis tag.[23,26] The PCR product was cloned into plasmid pCR2.1-TOPO (Invitrogen, Tokyo, Japan). The expression and purification system employed here was the same as that reported previously.[23] Cell-free expression was performed in the continuous exchange mode, using a dialysis membrane with a cutoff of 15 kDa (Spectrum, Rancho Dominguez, CA) to separate the reaction solution mixture (RM) from the feed solution mixture (FM). The components of each mixture have been described previously.[23] The template DNA used 4 μg/mL plasmid. Phosphatidylcholine from egg yolk (PC, 6.7 mg/mL) (Sigma, St. Louis, MO) and digitonin (0.4%, w/v) (Wako, Osaka, Japan) were added to the RM, and 100 μM all-*trans*-retinal (Sigma) was added to both the RM and FM solutions. The RM:FM volume ratio was 1:10. Synthesis reactions were performed at the 4.5 mL RM scale at 30 °C in a rotary shaker for 6 h, followed by ultracentrifugation (100000*g* for 30 min) of RM to separate ARII as a precipitant. The precipitate was washed with low-salt buffer [50 mM Tris-HCl (pH 6.8), 10 mM NaCl, and 10 mM EDTA] and then twice with high-salt buffer [50 mM Tris-HCl (pH 6.8) and 400 mM NaCl]. For purification, ARII was extracted into a high-salt buffer and 1% *n*-dodecyl β-D-maltoside (DDM) (Anatrace, Maumee, OH) at 4 °C for 1 h. After removal of the insoluble fraction by ultracentrifugation, the supernatant was subjected to nickel chelating chromatography (1 mL HisTrap HP, GE Healthcare, Tokyo, Japan). The unbound proteins were removed by washing the column with 10 column volumes of wash buffer [50 mM Tris-HCl (pH 6.8), 400 mM NaCl, 10% glycerol, 1 mM dithiothreitol, and 0.05% DDM] containing 20 mM imidazole. The bound protein was eluted with wash buffer containing 500 mM imidazole. The yield of ARII was 2.1 mg from 4.5 mL of the reaction mixture in the cell-free synthesis. The concentration was determined from the absorbance at 530 nm under an assumed extinction coefficient of 40000.

The 280 nm:532 nm absorbance ratio for this ARII sample was 1.68. In a previous report,[24] a lower ratio of 1.34 was obtained after purification using an N11 tag followed by gel filtration chromatography and removal of the tag. This sample showed one strong band and one faint band on sodium dodecyl sulfate−polyacrylamide gel electrophoresis. The faint band with a higher molecular weight was considered to be a dimer, suggesting that the purity of this sample was high. We should consider the contribution of the N11 tag to the 280 nm absorbance and estimated that the absorbance ratio for pure ARII with the tag was 1.41. Thus, this preparation contains small contaminants whose 280 nm absorbance may amount to 16%.

Flash Photolysis. The absorption changes of ARII were monitored after photoexcitation with an Nd:YAG laser pulse (532 nm, 7 ns) using the apparatus described previously.[27] The absorbance of the ARII samples used was ~0.5 at 530 nm, and the temperature was maintained at 20 °C. The medium consisted of 400 mM NaCl and 0.05% DDM (dodecyl β-D-maltoside), and the pH was adjusted to the desired values with MOPS or 6-mix buffer (citrate/MES/MOPS/HEPES/CAPS/CHES). The number of accumulations was 10. The global fitting analysis was performed for the data set measured from 320 to 700 nm with a 10 nm interval. The details of the procedure were reported previously.[28] Briefly, the data were fitted with a multiexponential function simultaneously for a data set of all wavelengths. The appropriate number of exponents was determined from the reductions in the standard deviation of the weighted residuals. Then further analysis proceeded according to the following irreversible sequential model: $P_0 \rightarrow P_1 \rightarrow P_2 \rightarrow \ldots \rightarrow P_0$, where P_0 represents the unphotolyzed original pigment and P_i represents the ith photochemically defined state.[29] This model contains only the forward reactions between P_i states. Thus, these P_i states may contain a few physically defined intermediates such as K−O when the reverse reactions exist between them. Using the fitting results, the time constant τ_i and the absorption differences between P_i and P_0 ($\Delta\varepsilon_i$) were calculated. Independently, the P_0 spectrum was obtained by subtracting the background scattering ($A + B/\lambda^4$; λ in nanometers) from the measured spectrum of the unphotolyzed state. Finally, the

dx.doi.org/10.1021/bi2009932 | *Biochemistry* 2011, 50, 8888–8898

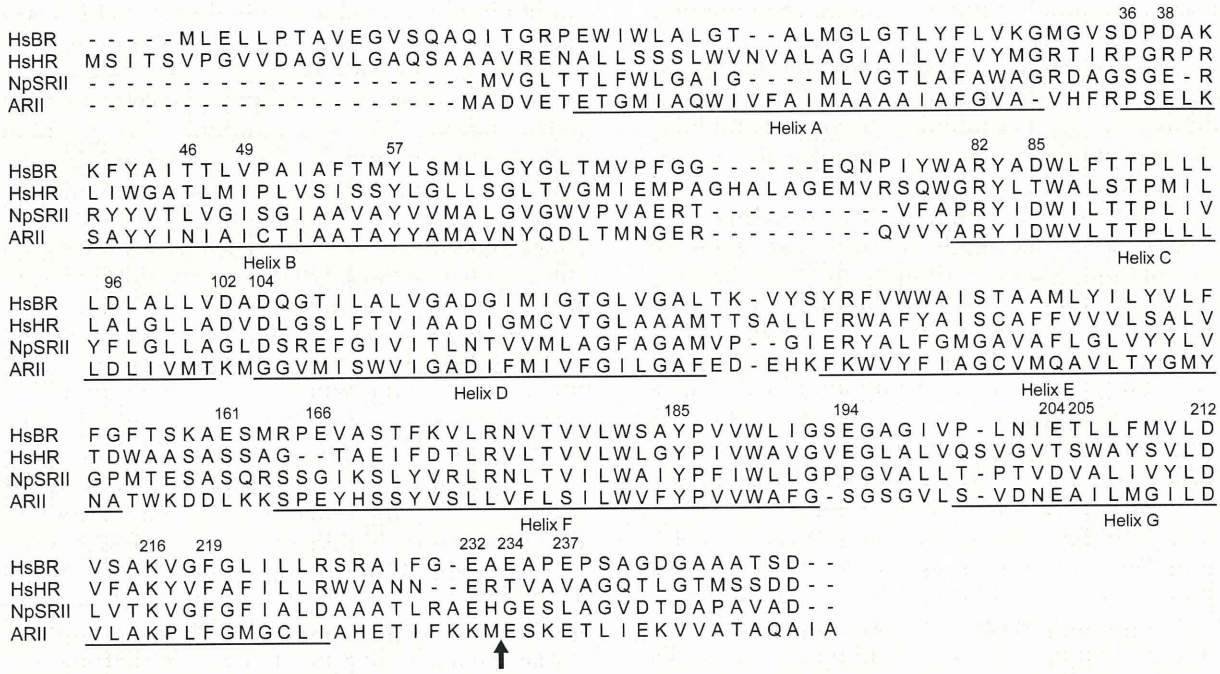

Figure 1. Comparison of the amino acid sequences of BR (from *Halobacterium salinarum*, HsBR), SRII (from *Natronomonas pharaonis*, also called *pp*R), HR (from *H. salinarum*), and ARII. The residue numbers are those of HsBR. The residues in HsBR that are essential for the proton pumping (at positions 82, 85, 96, 204, and 212 of BR) are all conserved in ARII except for that at position 194. However, other important residues are not necessarily conserved. Here, a truncated ARII is expressed from residue 1 to 229. The arrow indicates the truncated position.

absolute spectra of P_i states were obtained by adding the spectrum of P_0 to the absorption differences, $\Delta\varepsilon_i$. For details, see the paper by Chizhov et al.[29] as well as our previous studies.[27,28] The mathematical description was given by Sato et al.[27]

Measurements of Photoinduced Proton Transfer with an ITO Transparent Electrode and Pyranine. The photoinduced proton transfer was measured with an ITO (indium tin oxide) (Techno Print Co., Saitama, Japan) transparent electrode, which acts as a handy time-resolving pH sensor.[30] Purified ARII proteins fused with the N11 tag were reconstituted into PC at an ARII:PC molar ratio of 1:100 and suspended in distilled water.[31] The ARII suspensions of 100 μL with protein concentrations of ~10−30 μM were applied to the surface of ITO electrodes for ~60 min, followed by the evaporation of water under reduced pressure. By being sufficiently washed with distilled water, the unbound proteins were removed from the surface. The actinic light was obtained from a 300 W xenon lamp through a cold mirror, an IR cut filter (HA50) (Toshiba, Tokyo, Japan), and cutoff optical filters (>440 nm, Y44) (Toshiba). The sample was excited with pulse light using a mechanical shutter (duration of 2 ms). The electric signals from the ITO electrode were fed to a low-cut filter (0.08 Hz, MEG-1200) (Nihon Koden, Tokyo, Japan) to remove the fluctuation of the baseline. The buffer consisted of 400 mM NaCl and 1 mM 6-mix buffer (see Flash Photolysis). The buffer capacity of this 6-mix buffer was constant over the whole pH range examined. The ITO electrode deflection was proportional to the amounts of proton transferred by ARII. Details have been reported elsewhere.[30]

The proton transfer was also measured with a pH indicator dye pyranine (100 μM) (Invitrogen, Tokyo, Japan), and the method was essentially the same as reported previously.[30] The solubilized sample with 0.05% DDM was suspended in 400 mM NaCl buffered with 0.5 mM MOPS (pH 7.0).

RESULTS

Structure of the ARII Gene. ARII consists of 247 amino acid residues, and the levels of sequence identity were 53 and 24% for ARI and BR, respectively. Figure 1 shows the amino acid alignment of ARII with other typical microbial rhodopsins such as BR, HR, and SRII. Amino acid residues in BR that are essential for proton pumping are all conserved in ARII [Asp81 (corresponding to $Asp85^{BR}$), Asp92 ($Asp96^{BR}$), Arg78 ($Arg82^{BR}$), Glu199 ($Glu204^{BR}$), and Asp207 ($Asp212^{BR}$)], but $Glu194^{BR}$ is replaced with Ser, a nondissociable amino acid residue. In this work, we expressed a truncated ARII (from residue 1 to 229).

ARII Is a Light-Driven Proton Pump. As described later, the trace of flash-induced absorbance change at 520 nm (monitoring the original ARII) returned to the baseline at ~80 ms at pH 7−7.3 (see Figures 5 and 6). Thus, the photocycling rate is as fast as that of BR, and ARII is assumed to be a pump. Actually, a photoinduced electric current through an ARII-expressed oocyte membrane has been reported.[24] In addition, using an ITO-based, time-resolving detection method for pH change, light-induced proton uptake and release were observed (see Figures 5 and 7).

In spite of the identical function, λ_{max} of ARII, which is located around 530 nm, is largely blue-shifted from the value of 570 nm of BR. This difference might have originated from the different orientations between $Arg78^{ARII}$ and the corresponding $Arg82^{BR}$, because the X-ray crystal structure[24] revealed that $Arg78^{ARII}$ orients to EC. Ren et al. presented a theory based on quantum mechanics calculations that the blue shift of the absorbance maximum is caused by the orientation of the Arg residue corresponding to $Arg82^{BR}$ and concluded that this orientation is 70% responsible for the blue shift of SRII (λ_{max} ~ 500 nm), in which the corresponding Arg is oriented to EC.[32] Because the λ_{max} of ARII is 533.5 nm, which is closer to that of

dx.doi.org/10.1021/bi2009932 | *Biochemistry* 2011, 50, 8888–8898

BR than that of SRII, this theory may account well for the blue shift of the present pigment.

Photocycle at pH 7.0, a Physiological pH. The photocycle of ARII was investigated using the flash-photolysis technique at pH 7.0, a physiological pH. Figure 2 shows the light minus dark difference spectra in three time regions. Panel A shows the spectra from 8 to 57 μs, panel B those from 57 μs to 2.5 ms, and panel C those from 2.5 to 56 ms. Plots were started 8 μs after the laser flash because of the disappearance of the large scattering artifact from the flash. The times of 57 μs and 2.5 ms were chosen so that the characteristic intermediates reached the maximum accumulations. The medium contained 400 mM NaCl, 10 mM MOPS buffer (pH 7.0), and 0.05% DDM. Upon flash excitation, a photoproduct with a longer peak wavelength (~590 nm) appeared, followed by a decrease in this absorption band and a concomitant increase in the 400 nm band (panel A). This 400 nm band reached a maximum value of 57 μs. Judging from the time range and the location of the absorption band, the 590 nm band may be assigned to the K intermediate (abbreviated as K hereafter), although the time range of its appearance seems later than that of BR. The 400 nm band is the M intermediate (M hereafter). The decrease in the absorption at ~530 nm (increase in the magnitude of the negative band) after the flash (panel A) occurs because K has absorption in this wavelength region. Over time (panel B), the absorption of M decreases, but not completely, with a concomitant increase in the magnitude of another band with a longer wavelength. This band may be due to the N or O intermediate (abbreviated as N or O, respectively), which will be discussed later. O may have absorption around 550 nm, which extends to 660 nm (this will also be discussed later). At 2.5 ms in this panel (i.e., the last spectrum), the magnitude of this longer-wavelength band reaches its maximum. Panel C shows that M and the intermediate consisting of N and/or O decline completely to return to the original pigment.

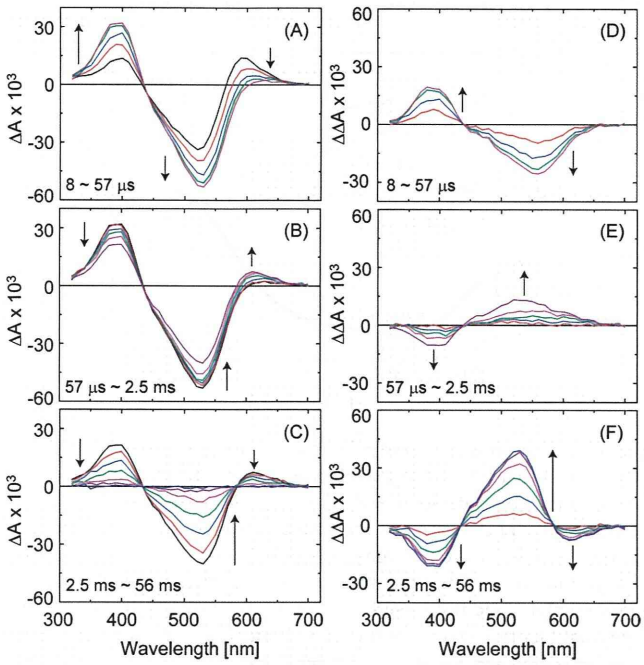

Figure 2. Flash-induced light minus dark difference spectra. Panels A–C show data for time ranges from 8 to 57 μs, from 57 μs to 2.5 ms, and from 2.5 to 56 ms, respectively. The upward arrow indicates the increase in the absorbance with time, while the downward arrow indicates its decrease. The times after the flash were 8.0, 13.0, 21.5, 35.5, and 57.4 μs for panel A; 57.4, 122, 262, and 548 μs and 1.17 and 2.51 ms for panel B; and 2.51, 4.16, 7.06, 11.7, 19.9, 33.8, and 56.1 ms for panel C. ARII (A_{530} ~ 0.5) solubilized with 0.05% DDM was suspended in 400 mM NaCl at pH 7, adjusted with 10 mM MOPS buffer. The temperature was 20 °C. Panel D is a difference spectrum that was redrawn with the spectrum at 8 μs in panel A as a new baseline. Panels E and F were similarly made from panels B and C with the spectrum at 57.4 μs and 2.51 ms as the new baselines, respectively.

To confirm this photocycle scheme, further analysis was performed. Figure 2D shows (double) difference spectra. The spectra in panel A are redrawn with the spectrum at 8 μs after the flash as a new baseline, which shows clearly that the intermediate with a longer λ_{max} (possibly K) converts to M with an isosbestic point on the baseline and that this photoproduct has a relatively wide absorption from 670 nm to at least 440 nm. The spectrum shape seems not to follow a Gaussian or skewed Gaussian distribution, which may be due to the presence of a putative L (see below). Figure 2E shows the set of the (double) difference spectrum where the spectrum at 57 μs in panel B is taken as a baseline, showing the decrease in M and a concomitant increase in the magnitude of a broad band with a longer wavelength, which may be assigned as N and/or O. The absorption in this band extends to as long as ~660 nm. Thus, it is assumed that this product contains O, which is the intermediate with the longest wavelength maximum among intermediates of the latter half of the BR photocycle. Figure 2F shows the set of (double) difference spectra, where the spectrum at 2.5 ms in panel C is taken as a baseline, showing that the disappearance of both M and the photoproduct with a longer wavelength (possibly O) occurs with an increase at 530 nm (recovery to the original ARII), which results in the completion of the photocycle. Note that it appears that M and O decay with almost the same time constant because there are two isosbestic points on the x-axis.

Next, a global fitting (see Materials and Methods) was performed. The standard deviation between the simulated and observed values became almost unity for a fitting equation of a sum of five exponential terms, indicating the existence of five photochemically defined states. Using the sequential irreversible model, we calculated the spectra of these states, which we designated as P_1–P_5. In this model, the photocycle can be represented by several irreversible, kinetically defined states (P_i), and P_i is assumed to decay by first-order kinetics. P_i contains a few physically defined intermediates such as K–O. The calculated spectra of these P species are shown in Figure 3, where P_0 denotes the spectrum of the original ARII. P_1 has a λ_{max} at 560 nm, which may be assigned as K, as described earlier. P_2 contains M and the absorption band with a longer wavelength (λ_{max} ~ 570 nm). Note the hollow at ~620 nm in Figure 2D. The identification of this longer-wavelength intermediate is not clear, but according to the sequence of intermediates observed in most of the microbial rhodopsins examined so far, it might be the L intermediate. However, ordinary L has its λ_{max} at a shorter wavelength. Thus, further study is needed. The spectra of P_1 and P_2 cross each other at ~440 nm, which is equal to the isosbestic point in Figure 2D, suggesting that the spectrum change shown in panels A and D (Figure 2) is the result of the exact conversion of P_1 to P_2 (with a time constant of 15 μs). During the P_2 to P_3 conversion (with a time constant of 0.1 ms), the decay of M is small and the λ_{max} of the photoproduct with a longer wavelength shifts to the shorter wavelength, indicating the appearance of new

dx.doi.org/10.1021/bi2009932 | Biochemistry 2011, 50, 8888–8898

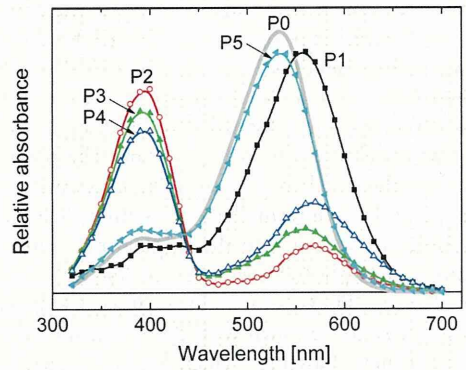

Figure 3. Spectra of photochemically defined photointermediates (P_1–P_5) calculated by a global fitting using an irreversible sequential model containing five successive intermediates (for details, see the text). The calculation was conducted for the difference spectra shown in Figure 2. P_0 denotes the spectrum of ARII, which was calculated by removing the scattering from the spectrum of ARII measured with a spectrophotometer (UV-1800) (Shimadzu, Kyoto, Japan).

intermediates. Next, P_3 is converted to P_4 with a time constant of 0.77 ms. In comparing the λ_{max} of the absorption bands at longer wavelengths (around 560–570 nm) between P_3 and P_4, we can see that the λ_{max} of P_4 is longer than that of P_3. This may imply the existence of both N and O in different ratios and that O has a longer λ_{max}. P_4 may contain a larger amount of O than P_3. P_4 is converted to P_5 with a time constant of 8 ms. The spectrum of P_5 is almost the same as that of ARII, and thus, P_5 is called ARII′. A similar intermediate was found in SRII.[33] Finally, P_5 decays to the original ARII with a time constant of 21 ms. Figure 4 shows the photocycle of ARII at 400 mM NaCl

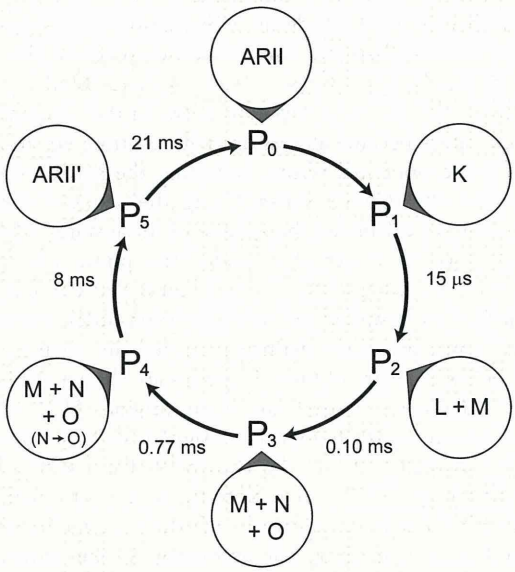

Figure 4. Proposed photocycle of ARII in 400 mM NaCl at pH 7 and 20 °C. Each P_i contains physically defined intermediates such as K–O, whose nomenclature followed that of BR. ARII′ is an intermediate whose structure is considered to be similar to that of the original ARII. Note that P_4, the latter part of the intermediate, contains both M and O, suggesting the existence of the O → M reverse reaction via N. The difference between P_3 and P_4 is due to the content of O in P_4 being larger than that of P_3.

(pH 7.0) in the presence of 0.05% DDM at 20 °C. As described above and shown in Figure 4, M remains in the latter half of the photocycle, and P_4 has both M and O (Figures 3 and 4), which may be interpreted as the existence of a reverse-directed change from O to M and the forward reaction, assuming that the rates of the reverse changes may be larger than or comparable to those of the forward reaction.

Figure 5 shows the flash-induced pyranine absorbance change (indicating a pH change) and the absorbance changes

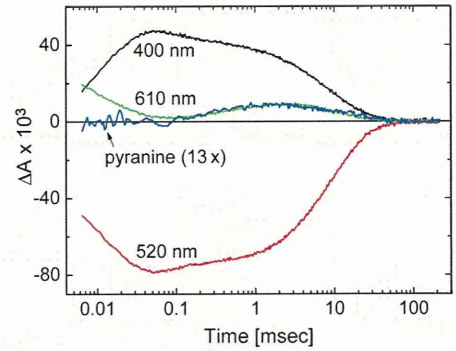

Figure 5. Proton uptake and release coincide with the formation and decay of O. Flash-induced absorbance changes at 400, 520, and 610 nm monitor the change in M, the original ARII with N, and O, respectively. The pyranine absorbance change indicates the pH change, and the 13-fold magnified signal is overlaid on the 610 nm change monitoring O. The pyranine concentration was 100 μM. The experimental conditions were the same as those described in the legend of Figure 2 except for the dilute buffer concentration (0.5 mM).

of three typical wavelengths (400, 610, and 520 nm) that monitor mainly M, O, and the original pigment, respectively. The pH was 7.0. The 610 nm absorbance changes reflect mainly the change in O, as described below. This figure reveals that the proton uptake occurs first, followed by release, and the proton transfer completely matches the 610 nm absorbance change. Obviously, the 400 nm absorbance change monitors only the change in M, and Figure 5 reveals that the proton uptake never occurs during the decay or formation of M. Furthermore, the proton release may not occur during ARII′ decay because this intermediate is very similar to the original ARII. Therefore, the 610 nm absorbance change can be regarded as the change of O, and thus, the photocycle and the proton transfer of ARII (at pH 7.0) are as shown in Scheme 1.

Scheme 1. Proposed Photocycle of ARII at 400 mM NaCl, pH 7, and 20 °C

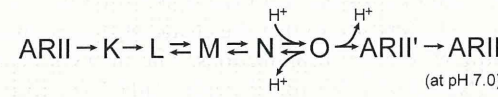

Here, the respective rate constants of conversions among M, N, and O could not be determined, but those of P_i to P_{i+1} were determined. Their values at pH 7.0 are shown in Figure 4.

Photocycle at Varying pH Values. The photocycle at varying pH values was examined, and the results are shown in Figure 6. Here, the three typical wavelengths of monitoring light were employed (400, 610, and 520 nm). First, the change in the 400 nm absorbance (monitoring M) was observed. In acidic media (pH 4.1), the decay of M is so fast that it disappears as early as 0.1 ms, and this rate is ~10-fold faster than that of BR.[2,3] The decay seems to follow a single component, suggesting that the equilibrium between M and N

dx.doi.org/10.1021/bi2009932 | Biochemistry 2011, 50, 8888–8898

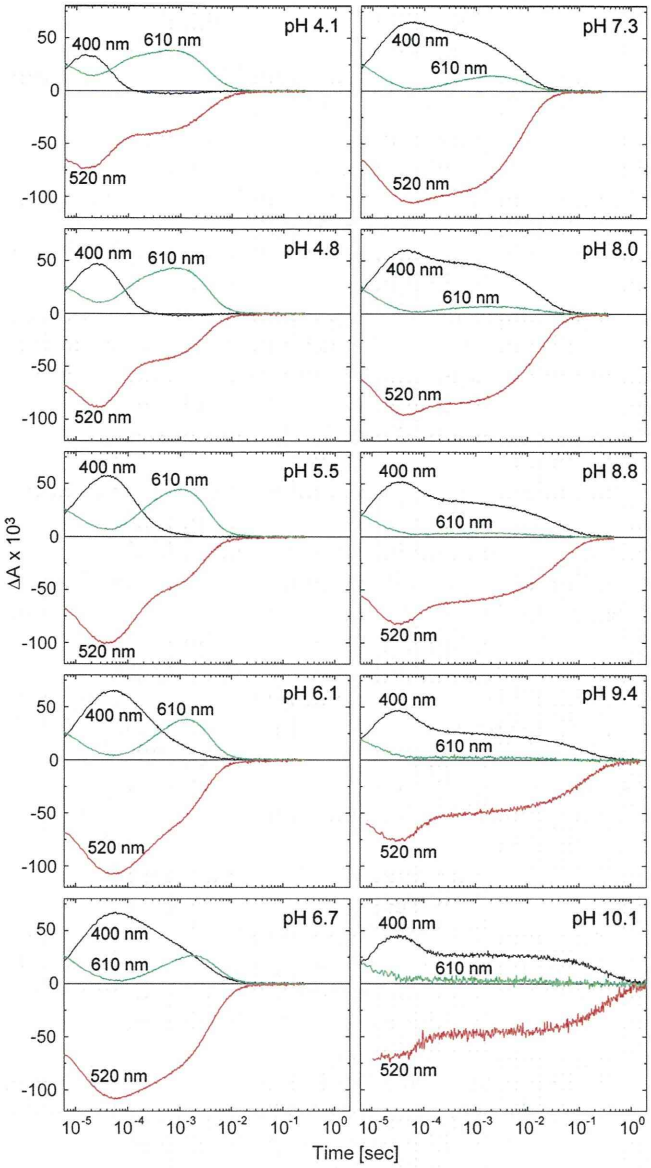

Figure 6. Flash-induced absorbance changes at selected wavelengths (400, 520, and 610 nm) at varying pH values. The intermediates monitored by these wavelengths are named in Figure 5. The buffer used was 2 mM 6-mix buffer (citrate/MES/MOPS/HEPES/CAPS/CHES). The other experimental conditions were the same as those described in the legend of Figure 2.

(see Scheme 1) is not prominent because of the first decay of N. With an increase in pH, the decay becomes slower and follows a multicomponent decay (a biphasic decay at pH 5.5–6.7 and a triphasic decay at pH 7.3–10.1). Note that, around pH 5.5, the manner of decay changes from mono- to biphasic, suggesting that the pK_a of a certain amino acid residue is at pH ~6, which controls the decay of a certain photointermediate. The delay of M decay does not necessarily mean that of M decay itself because, as shown above, the intermediates are connected to each other by the forward and backward reactions. Under the alkaline conditions, the decay of M becomes triphasic, which may be due to the existence of three intermediates. The earliest decay of M seems to be pH-independent (~0.1 ms), suggesting the existence of pH-independent M decay. In an alkaline solution, the N → O process may be very slow because of the low proton concentration in media, so that we may observe only the equilibrium complex of M and N, whose decay follows the decay constant of the N → O process (very slow). In fact, this figure reveals the quasi-steady state at pH >9.4.

Next, the 610 nm change that monitors mainly O was observed. In acidic solutions (pH 4.1–6.1), M decay seems to match O formation, and furthermore, its decay seems to match the recovery of the original pigment. On the other hand, in neutral or weakly alkaline solutions, late M and O seem to decay simultaneously, which coincides with the recovery of the original pigment. In more alkaline solutions (pH 8.8–10.1), O does not appear. The rise and decay of the 610 nm band in a very early time range (approximately several tenths of microseconds) are not due to O but K. The fact that the formation of O is not observed may be due to the slow decay of its precursor, N. These observations suggest that (1) there are M ← N and N ← O reverse reactions and (2) there are pH-dependent processes.

The global fitting was also done for pH 5.0 and 8.6 as well as pH 7.0. Five intermediates were sufficient to simulate the flash-photolysis data, and the spectra of these intermediates (data not shown) were similar to those in Figure 3. However, the following observations were also made. (1) In acidic solutions, there was no M in the later intermediates of P_3 and P_4 because of the rapid decay of M, as shown in Figure 6. (2) Even in acidic solutions, N appeared, which may have been because of the rapid reverse reaction from O to N. (3) On the other hand, in alkaline solutions, the spectra of the 600–700 nm regions in P_3 and P_4 were diminished, implying that O did not appear, which was consistent with Figure 6. The values for the lifetime evaluation are listed in Table 1. Those of P_1 and P_2 were

Table 1. Lifetimes of P_i Intermediates at Varying pH Values[a]

	pH 5.0[b]	pH 7.0	pH 8.6[b]
P_1	0.014	0.015	0.014
P_2	0.072	0.097	0.053
P_3	0.76	0.77	3.13
P_4	2.50	7.96	26.3
P_5	17.2	20.9	115.4

[a]Units of milliseconds. [b]For pH 5.0 and 8.6, 10 mM 6-mix buffer was used, and the other experimental conditions were the same as those for pH 7.0 (Figure 2).

essentially pH-independent. On the other hand, with an increase in pH, the values for the lifetimes of P_3–P_5 increased appreciably. The increase in the lifetimes of P_3 and P_4 (especially P_4) may have been due to the slow proton uptake at N (see Discussion). Note that P_3 and P_4 contain N. The reason for the pH dependence of P_5 (ARII′) was not clear, but it suggested the H^+ association of some amino acid(s) during the conversion of ARII′ to the original ARII.

Proton Transfer during the Photocycle: ITO Signal versus pH of the Medium. Figure 6 indicates that some pH-dependent transitions of intermediates occurred. In addition, ARII is a light-driven proton pump. Then the next problem is to determine which process is coincident with the uptake and release of protons. The time-dependent proton transfer was measured using an ITO method.[30] Figure 7 shows traces of the time-dependent voltage changes of the ITO electrode (ΔVoltage) at varying pH values. The ΔVoltage values are proportional to the pH changes, and under the conditions in which the pH changes are small and the buffer capacity is

dx.doi.org/10.1021/bi2009932|*Biochemistry* 2011, 50, 8888–8898

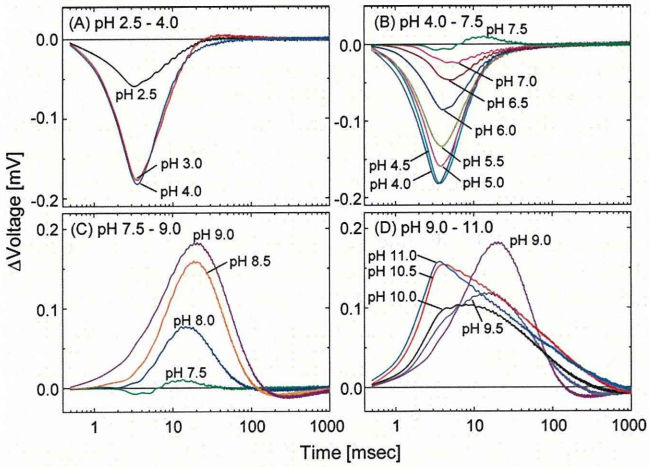

Figure 7. Proton transfer measured with a transparent ITO electrode. The downward (negative) deflection indicates the alkalization in the medium, i.e., uptake of a proton by ARII, while the upward shift indicates proton release. The medium was 400 mM NaCl buffered with 1 mM 6-mix buffer. Details are given in the text.

constant for all pH values (these are fulfilled in this experiment), the changes are proportional to the numbers of proton moved by the photoinduced transfer. Contrary to the pyranine changes in Figure 5, the downward shift indicates proton uptake and the upward shift indicates proton release. In Figure 8, the peak values of Figure 7 are plotted versus pH,

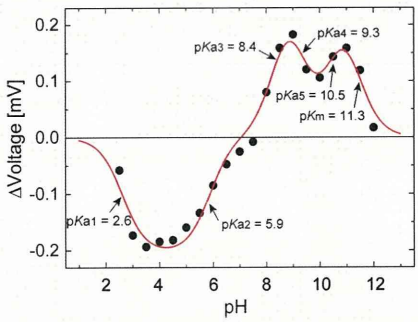

Figure 8. Peak values in Figure 7 plotted vs pH. The discussion in the text separated the pH values into six regions. These were the pH ranges of (1) 2.5–4, (2) 4–7, (3) 7–9, (4) 9–10, (5) 10–11, and (6) >11. The solid line shows the curves simulated using an equation in the text. The estimated pK_a values are shown in the figure.

where the negative values indicate the first proton uptake and the positive values indicate the first proton release. These figures show that, below pH 7, proton uptake occurs first, followed by release. On the other hand, above pH 7, the sequence of the proton movement is reversed. This behavior is very similar to that of BR (see Figure 7 of ref 30) except for two points. (1) The pH at which proton uptake converts to release is ~7 for ARII and ~5 for BR. (2) There is a peak at pH 11 for ARII, while that of BR is a monotonous decrease.

DISCUSSION

Photocycle and Proton Transfer. As described above, the photocycle at pH 7.0 was examined in detail (Figure 2). Intermediates K–O and ARII′ were found, similar to BR. On the other hand, formation of M and O occurred in less than 0.1 and 2 ms, respectively, much faster than the corresponding formations for BR (Figure 5).[3,34] In addition, there were pronounced N → M and O → N reverse reactions. Although the reverse reactions are present in BR,[3,34] these rates of ARII seem much larger than those of BR. Thus, P_4, interestingly, was composed of a mixture of M–O (Figure 4). The existence of the equilibrium mixture of intermediates was predicted by Hegemann and colleagues[20] from the kinetic analysis of the flash-induced electric current through an oocyte membrane with AR that was homologous to but different from the present ARII. Chizhov et al.[29] analyzed the photocycle of BR using the irreversible sequential model, which was the same as that used here, and their analysis did not involve a photochemically defined intermediate with the copresence of M and O; P_3 and P_4 of ARII contain both M and O in addition to N. The copresence of M and O may be due to the reverse reaction from O to M.

The rapid reverse reaction might be disadvantageous for ion pumping. However, it may be possible because the photocycling rate is as fast as that of BR at neutral pH. For example, formation of O of ARII was very fast, as described above (Figure 6). In addition, the presence of the one-way (irreversible) conversion of O to ARII′ and of ARII′ to the original pigment may serve to promote the one-way reaction. For BR, there are at least two M intermediates, at one of which (M1) BR is open to the extracellular (EC) and at the other of which (M2) BR is open to the cytoplasmic (CP) channel.[3,34] The switch from M1 to M2 is indispensable for pumping.[3] Then a question for a future investigation is whether M1 and M2 exist in ARII.

The rates of the forward and reverse reactions may be dependent on pH because the formation and/or decay of a certain intermediate may be associated with proton transfer. Here, the transfer was measured with a transparent ITO electrode.[30] According to Figure 8, the pH range is divided into six regions for the discussion of the plausible mechanism of proton transfer in each region.

pH Region between pH 2.5 and 4.0. In this pH region, proton uptake occurs first, followed by release. The amounts of uptake increase with an increase in pH. The counterion of the Schiff base ($Asp81^{ARII}$) should receive a proton from the protonated Schiff base upon illumination, which leads to M. In acidic solutions (pH 1 or 2), $Asp81^{ARII}$ may be protonated in the dark and this form cannot accept the proton, and thus, proton transfer is not initiated. Thus, the curve in this region is considered to be reflected by the pK_a of $Asp81^{ARII}$ in the dark [2.6 (see below)]. The amounts of flash-induced M also increased with an increase in this pH range (data not shown). During the formation of M, the proton on the Schiff base is transferred to the deprotonated $Asp81^{ARII}$ while the Schiff base is deprotonated. The deprotonated Schiff base regains a proton from $Asp92^{ARII}$, a proton donor residue corresponding to $Asp96^{BR}$, which leads to N. In low-pH media, deprotonated $Asp92^{ARII}$ becomes protonated by the entry of a proton from the outside medium (which leads to O). This process is faster because of the low pH than that of release of a proton from the protonated $Asp81^{ARII}$ (O decay).

pH Region between pH 4.0 and 7.0. A comparison between Figures 6 and 7B indicates that the proton release matches the 610 nm (O) decay of the flash-photolysis data well. Because of the low fidelity of the time resolution of ITO in the time range of several milliseconds, the matching between the 610 nm (O) rise and ITO data is not good. Figure 5, however, shows that uptake and release of protons occur during the

dx.doi.org/10.1021/bi2009932|*Biochemistry* 2011, 50, 8888–8898

formation and decay of O, respectively, at pH 7.0. In this pH region, the magnitudes of the rate of uptake decrease with an increase in pH, but uptake occurs first. This behavior is similar to that of BR (see Figure 7 of ref 30). This behavior of BR is interpreted as an initiation of the release of a proton from the proton-releasing complex during the formation of O.[30,34] The proton-releasing residue of our ARII may be Glu199^{ARII}, which corresponds to Glu204^{BR}, although the residue corresponding to Glu194^{BR}, one of the members of the proton-releasing complex, is Ser^{ARII}, a nondissociable residue (Figure 1). For proton release, the necessity of the simultaneous existence of two dissociable residues at these positions does not hold because Asp193$^{NpSRII\ (ppR)}$ is a proton-releasing residue[31] in spite of the fact that the counterpart of Glu194^{BR} is Pro, a nondissociable residue (Figure 1). To check whether a proton is released from Glu199^{ARII} in this pH region, the proton transfer of the E199Q mutant was examined and was found to exhibit almost the same behavior below pH 7 (data not shown and manuscript in preparation), although a pH decrease of ~0.5 was observed. Thus, the decrease in the rate of the first proton uptake with an increase in pH (Figure 8) was not due to the initiation of the release of a proton from E199^{ARII} at O.

Careful inspection of Figure 7B indicates that, with an increase in pH, (1) the proton uptake rate (especially above pH 6) becomes slower and (2) the peaks shift gradually to the right. These observations indicate that the pK_a of Asp92^{ARII} during N decay may range from pH ~6 to ~6.5, which would result in the slower proton uptake in the pH region above this pK_a, because the proton uptake during N decay may proceed via the protonation of Asp92^{ARII}. The slower decay of M with an increase in pH [>6.0 (Figure 6)] may support this hypothesis, as well, because the presence of the N → M reaction implies that the slow decay of N results in the slow decay of M. On the other hand, the rate of decay of O may be relatively pH-independent, as is assumed from the flash-photolysis data in this pH range (Figure 6), which is consistent with the relatively pH-independent proton release shown in Figure 7B. Therefore, N decay (O rise) becomes slow above a pH of the pK_a of Asp92^{ARII}. At pH values above this pK_a, the observed rate of proton uptake, which is a summation from all molecules, becomes smaller in magnitude and lasts for a longer time, obeying a time constant of N decay. As described above, O decay is relatively pH-independent, which indicates pH-independent proton release. Then the overall signal of the proton uptake becomes small with an increase in pH, which is an interpretation of the proton transfer in this pH region. The presence of two kinds of molecules with different proton transfer timing is clearly shown in the ITO trace at pH 7.5 (Figure 7). The amounts of O decrease as the pH increases (Figure 6), but the pH dependence of the decrease seems small in comparison with that of pH 4–7 of the ITO signal (Figure 8). This may be due to the existence of M–O complexes and the slow decays of P_3 and P_4 in an alkaline solution (Table 1), although O disappeared in more alkaline solutions.

Analysis of the proton uptake kinetics in panel B in Figure 7 using the Henderson–Hasselbalch equation gave a pK_a of 6.3 (data not shown), although the fidelity of the time response of the ITO electrode in this time range (several milliseconds) is not good.[30] However, this value is reasonable and supportive of the mechanism described above because the fitting of the curve in Figure 8 gave a pK_a of 5.9 (see below). Thus, a pK_a of 6.3 or 5.9 may be assumed for Asp92^{ARII}. The corresponding value of Asp96^{BR} is ~7.8.[30,34] The lower value of ARII suggests the hydrophilic nature in the CP during N decay. On the other hand, the pK_a of Asp92^{ARII}, a proton donor in the dark, is very high because the presence of a very fast M decay component (~0.1 ms) for the whole pH region (Figure 6) suggests the capacity for donation of protons to the deprotonated Schiff base even at pH 10.

pH Region from pH 7.0 to 9.0. In this pH region, proton release occurs first, followed by proton uptake. During M decay, the deprotonated Schiff base receives a proton from Asp92^{ARII}, and N is formed. Because the pK_a of Asp92^{ARII} at N is 6.3 or 5.9 (see above), the lifetime of N in this pH range should be very long, which may give rise to a very long 400 nm decay (Figure 6) and suggests the formation of the mixture of M and N. Consequently, a small 610 nm component (O intermediate) is found (Figure 6).

The question to be addressed is the residue from which the proton is first released. The most probable residue is Glu199^{ARII} (corresponding to Glu204^{BR}), as described above. Hence, experiments were performed using the E199Q^{ARII} mutant. The peak located from pH 7 to 10 in Figure 8 disappeared completely (manuscript in preparation), revealing clearly that the proton is released first from Glu199^{ARII}. The pK_a of this residue upon release of the proton is located in this pH region and was determined to be 8.4 (see below). Hegemann and co-workers[20] proposed that the pK_a of the proton-releasing residue is ~9 based on the oocyte experiments with an AR that was homologous but not identical to our ARII. As the pH increases, the fraction of the fast proton-releasable molecule increases. The other molecules show the first proton uptake as in the lower-pH region. Then the time to start the upward shift (proton release) becomes earlier with an increase in pH (Figure 7C).

Although the ITO electrode does not respond as quickly as 0.1 ms,[30] these data may not indicate that the proton is released during the formation of M as is the case for BR.[3,34] In Figure 7D, the faster proton release occurs at the higher pH, revealing that the proton release in this pH range is slow. The correlation between the formation of M and proton release should be investigated in the future. If proton release does not occur with the formation of M, why is proton release slow in comparison with that of BR? According to the X-ray crystal structure,[24] Arg78^{ARII} (corresponding to Arg82^{BR}) in the dark orients to EC, suggesting that there is no flip-flop motion like that seen for BR. However, this cannot be the sole reason, because phospholipid-reconstituted NpSRII (*p*pR) showed proton release prior to M decay and because Arg72^{NpSRII} [corresponding to Arg78^{ARII} and Arg82^{BR} (see Figure 1)] also orients to EC in the dark.[35−37] The pK_a of the proton-releasing residue at the ground state in NpSRII differs from that in ARII, although the orientations of the Arg side chains are similar to each other. One possible reason for this is that a water molecule such as that which interacts with Asp193^{NpSRII} and Arg72^{NpSRII} may not exist around Glu199 and Arg78 in ARII.[24] We surmised previously that this may disrupt the formation of the low-barrier hydrogen bond at Glu199, resulting in "late proton release".[24] Further study of this phenomenon is necessary.

The corresponding value of BR is 6.1,[30,34] while that of ARII is 8.4. In addition, the value of the BR-like protein from a salt lake in Tibet was reported to be 8.3.[38] The molecular factor for determining this pK_a value should be studied in the future.

pH Region from pH 9.0 to 10. In this region, the magnitude of the ITO signal deceases with an increase in pH (Figure 8). As described above, the fast proton transfer is associated with

dx.doi.org/10.1021/bi2009932|*Biochemistry* 2011, 50, 8888–8898

Glu199^{ARII}. This decrease may be ascribed to the deprotonation of Glu199^{ARII} in the dark. When this residue has no dissociable proton in the dark, it can no longer release protons during the photocycle. As described below, the pK_a was estimated to be 9.3, which was assigned to the pK_a of Glu199^{ARII} in the dark. The fraction of the proton-release-disabled molecule (having deprotonated Glu199^{ARII} in the dark) increases with an increase in pH, and the magnitude of the first proton release decreases. For the proton-release-disabled molecule, proton release might occur from the counterion of Asp81^{ARII} during O decay, before which proton uptake might occur during the very slow N decay.

pH Region from pH 10 to 11. Surprisingly, the magnitude of proton release again increases with an increase in pH (Figure 8). The exact mechanism is not known at present. However, it is feasible that a residue (abbreviated as H-X) may work as a proton-releasing residue that is different from Glu199^{ARII} and Asp81^{ARII}. The fast release of a proton from Asp81^{ARII} is difficult to assume because M formation was observed. A similar phenomenon was observed for proteorhodopsin.[30] A candidate of this residue may be either Arg78^{ARII} or the Schiff base itself. The identification of H-X is a subject for a future investigation. The proton uptake process is very slow (Figure 7D), and the amount of M remains almost constant for a long time with no appearance of O, which suggests the very slow decay of an equilibrium complex of M and N.

pH Region above pH 11. Denaturation of ARII occurred. Once the sample was subjected to this condition, the signals of both flash photolysis and ITO diminished (data not shown). Thus, the pK_a value in this region is pK_m, indicating that its meaning is different from that of the normal pK_a.

Estimation of pK_a Values. On the basis of the discussion above, the fitting equation for the ITO data (Figure 8) should be as follows:

$$\Delta\text{Voltage} = -\frac{A}{(1+10^{pK_{a1}-pH})(1+10^{pH-pK_{a2}})} + \frac{B}{(1+10^{pK_{a3}-pH})(1+10^{pH-pK_{a4}})} + \frac{C}{(1+10^{pK_{a5}-pH})(1+10^{pH-pK_m})}$$

where A, B, and C are constants determining the magnitude of the deflection and pK_{ai} (i = 1−5) and pK_m represent the pK_a value of the ith phase and the pH giving half of the denaturation in Figure 8, respectively. Because the counterion of the Schiff base, Asp81^{ARII}, should be deprotonated in the dark so that protons can be accepted from the Schiff base, the second and third terms should contain this factor of pK_{a1}. However, in the pH range of 2−6 in Figure 8, this condition should be automatically fulfilled because the pK_{a1} is 2.6. The simulated curve is drawn with a solid line in Figure 8. The estimated pK_{ai} (i = 1−5) values and pK_m are 2.6, 5.9, 8.4, 9.3, 10.5, and 11.3, respectively.

The accuracy of the estimated pK_a values should be discussed. The peak values of Figure 7 were plotted and analyzed. The peak time and its magnitude were dependent on both of the on- and off-time constants. Therefore, the pK_a values estimated by this method may contain some error, because the decay or rise process was not analyzed solely. However, the values for the BR estimated previously[30] were approximately equal to those reported by different spectroscopic methods. In addition, Wu et al.[38] estimated the pK_a value of the proton-releasing residues of BR and BR-like rhodopsin from Tibet using ITO. They derived a rigorous theoretical equation for the estimation and obtained 5.6 ± 0.1 as the pK_a of the proton-releasing complex. This method gave a value of 6.1.[30] Other investigators reported a value of ~5.8 (see ref 33 and the references cited therein). Wu et al.[38] employed our peak method for the determination of the pK_a of the D96N^{BR} mutant and obtained a value of 5.82, which is similar to that obtained with the rigorous treatment. Therefore, in consideration of their convenience, simplicity, and accuracy, the ITO method and the analysis approach presented herein can be considered powerful and effective tools.

■ CONCLUSIONS

In this paper, the appreciably fast reverse reactions in ARII are shown, such that the photochemically defined photointermediates have an equilibrium mixture of physically defined intermediates such as M−O. The X-ray structure[24] showed that Arg78^{ARII} orients to EC in the dark, in contrast to BR. However, this orientation is not responsible for the existence of the fast reverse reaction because the corresponding Arg of NpSRII also orients to EC,[35−37] but the reverse reactions of NpSRII are negligible.[14] The large reverse reaction in BR was reported in a mutant.[39] The molecular interpretation of the existence of such fast backward reactions should be a topic of further research. The pK_a values for some amino acids were estimated by the ITO method.[30] The pK_a value of the proton-releasing residue at M (8.4) was larger than that of BR (6.1) by 2.3 units.[30,40] In addition, residue H-X, which releases protons under highly alkaline conditions, should be identified. For elucidation of the proton-pumping mechanism, a higher-resolution X-ray crystal structure that can reveal the location of water molecules is needed. Improvement of the crystal of ARII is now underway.

■ AUTHOR INFORMATION

Corresponding Author

*S.Y.: telephone, +81-45-503-9196; fax, +81-45-503-9195; e-mail, yokoyama@biochem.s.u-tokyo.ac.jp. N.K.: telephone and fax, +81-89-926-7138; e-mail, nkamo@cc.matsuyama-u.ac.jp.

Funding

This work was supported by the Targeted Proteins Research Program (TPRP). Additional support was provided by the National Research Foundation of Korea (NRF 331-2008-1-C00242), the Development of Marine-Bioenergy Program funded by the Ministry of Land, Transport and Maritime Affairs of the Korean Government, and the second stage of the Brain Korea 21 Graduate Fellowship Program (to S.Y.K.). This work was also supported by grants from the Japanese Ministry of Education, Culture, Sports, Science, and Technology to K.S. (19770136) and N.K. (22590049).

■ ABBREVIATIONS

AR, *Acetabularia* rhodopsin; BR, bacteriorhodopsin; CAPS, *N*-cyclohexyl-3-aminopropanesulfonic acid; CHES, *N*-cyclohexyl-2-aminoethanesulfonic acid; CP, cytoplasmic channel; DDM, dodecyl β-D-maltoside; EC, extracellular channel; HsSRII, sensory rhodopsin II from *H. salinarum* (also phoborhodopsin); HR, halorhodopsin; HEPES, 4-(2-hydroxyethyl)-1-piperazineethanesulfonic acid; ITO, indium tin oxide; MES, 2-(*N*-morpholino)ethanesulfonic acid; MOPS, 3-(*N*-morpholino)-propanesulfonic acid; NpSRII, sensory rhodopsin II from *N.*

dx.doi.org/10.1021/bi2009932 | *Biochemistry* 2011, 50, 8888–8898

pharaonis (also *p*pR); SRI, sensory rhodopsin I; SRII, sensory rhodopsin II.

REFERENCES

(1) Spudich, J. L., and Jung, K.-H. (2005) Microbial rhodopsin: Phylogenetic and functional diversity. In *Handbook of photosensory receptors* (Briggs, W. R., and Spudich, J. L., Eds.) pp 1–23, Wiley-VCH Verlag, Weinheim, Germany.

(2) Haupts, U., Tittor, J., and Oesterhelt, D. (1999) Closing in on bacteriorhodopsin: Progress in understanding the molecule. *Annu. Rev. Biophys. Biomol. Struct. 28*, 367–399.

(3) Lanyi, J. K. (2006) Proton transfers in the bacteriorhodopsin photocycle. *Biochim. Biophys. Acta 1460*, 220–229.

(4) Mukohata, Y., Ihara, K., Tamura, T., and Sugiyama, Y. (1999) Halobacterial rhodopsins. *J. Biochem. 125*, 649–657.

(5) Lanyi, J. K. (1981) Halorhodopsin: A 2nd retinal pigment in *Halobacterium halobium*. *Trends Biochem. Sci. 6*, 60–62.

(6) Essen, L. O. (2002) Halorhodopsin: Light-driven ion pumping made simple? *Curr. Opin. Struct. Biol. 12*, 516–522.

(7) Bogomolni, R. A., and Spudich, J. L. (1982) Identification of a third rhodopsin-like pigment in phototactic *Halobacterium halobium*. *Proc. Natl. Acad. Sci. U.S.A. 79*, 6250–6254.

(8) Spudich, J. L., and Bogomolni, R. A. (1984) Mechanism of color discrimination by a bacterial sensory rhodopsin. *Nature 312*, 509–513.

(9) Hazemoto, N., Kamo, N., Terayama, Y., Kobatake, Y., and Tsuda, M. (1983) Photochemistry of two rhodopsinlike pigments in bacteriorhodopsin-free mutant of *Halobacterium halobium*. *Biophys. J. 44*, 59–64.

(10) Takahashi, T., Tomioka, H., Kamo, N., and Kobatake, Y. (1985) A photosystem other than P370 also mediates the negative phototaxis of *Halobacterium halobium*. *FEMS Microbiol. Lett. 28*, 161–164.

(11) Wolff, E. K., Bogomolni, R. A., Scherrer, P., Hess, B., and Stoeckenius, W. (1986) Color discrimination in halobacteria: Spectroscopic characterization of a second sensory receptor covering the blue-green region of the spectrum. *Proc. Natl. Acad. Sci. U.S.A. 83*, 7272–7276.

(12) Spudich, E. N., Sundberg, S. A., Manor, D., and Spudich, J. L. (1986) Properties of a second sensory receptor protein in *Halobacterium halobium* phototaxis. *Proteins 1*, 239–246.

(13) Marwan, W., and Oesterhelt, D. (1987) Signal formation in the halobacterial photophobic response mediated by a 4th retinal protein (P480). *J. Mol. Biol. 195*, 333–324.

(14) Kamo, N., Shimono, K., Iwamoto, M., and Sudo, Y. (2001) Photochemistry and photoinduced proton-transfer by *pharaonis* phoborhodopsin. *Biochemistry (Moscow, Russ. Fed.) 66*, 1277–1282.

(15) Nagel, G., Ollig, D., Fuhrmann, M., Mustl, A. M., Bamberg, E., and Hegemann, P. (2002) Channelrhodopsin-1: A light-gated proton channel in green algae. *Science 296*, 2395–2398.

(16) Sineshchekov, O. A., Jung, K.-H., and Spudich, J. L. (2002) Two rhodopsins mediate phototaxis to low- and high-intensity light in *Chlamydomonas reinhardtii*. *Proc. Natl. Acad. Sci. U.S.A. 99*, 8689–8694.

(17) Suzuki, T., Yamasaki, K., Fujita, S., Oda, K., Iseki, M., Yoshida, K., Watanabe, M., Daiyasu, H., Toh, H., Asamizu, E., Tabata, S., Miura, K., Fukuzawa, H., Nakamura, S., and Takahashi, T. (2003) Archaeal-type rhodopsins in *Chlamydomonas*: Model structure and intracellular localization. *Biochem. Biophys. Res. Commun. 301*, 711–717.

(18) Schilde, C. (1968) Rapid photoelectric effect in the alga *Acetabularia*. *Z. Naturforsch., B: Chem. Sci. 23*, 1369–1376.

(19) Henry, I. M., Wilkinson, M. D., Hermandez, J. M., Schwarz-Sommer, Z., Grotewold, E., and Mandoli, D. F. (2004) Comparison of EST's from juvenile and adult phases of the giant unicellular green algae *Acetabularia acetabulum*. *BMC Plant Biol. 4*, 3–14.

(20) Tsunoda, S. P., Ewers, D., Gazzarrini, S., Moroni, A., Gradmann, D., and Hegeman, P. (2006) H^+-pumping rhodopsin from the marine alga *Acetabularia*. *Biophys. J. 91*, 1471–1479.

(21) Hagedom, R., Gradmann, D., and Hegemann, P. (2008) Dynamics of voltage profile in enzymatic ion transporters, demonstrated in electrokinetics of proton pumping rhodopsin. *Biophys. J. 95*, 5005–5013.

(22) Lee, K. A., Kim, S. Y., Choi, A. R., Kim, S. H., Kim, S. J., and Jung, K.-H. (2010) Expression of membrane protein and photochemical properties of two *Acetabularia* rhodopsins. Abstract of the 14th International Conference on Retinal Proteins, P-23, Santa Cruz, CA, August 2–6.

(23) Shimono, K., Goto, M., Kikukawa, T., Miyauchi, S., Shirouzu, M., Kamo, N., and Yokoyama, S. (2009) Production of functional bacteriorhodopsin by an *Escherichia coli* cell-free protein synthesis system supplemented with steroid detergent and lipid. *Protein Sci. 18*, 2160–2171.

(24) Wada, T., Shimono, K., Kikukawa, T., Hato, M., Shinya, N., Kim, S. Y., Kimura-Someya, T., Shirouzu, M., Tamogami, J., Miyauchi, S., Jung, K.-H., Kamo, N., and Yokoyama, S. (2011) Crystal structure of the eukaryotic light-driven proton pumping rhodopsin, *Acetabularia* rhodopsin II, from marine alga. *J. Mol. Biol. 411*, 986–998.

(25) Yabuki, T., Motoda, Y., Hanada, K., Nunokawa, E., Saito, M., Seki, E., Inoue, M., Kigawa, T., and Yokoyama, S. (2007) A robust two-step PCR method of template DNA production for high-throughput cell-free protein synthesis. *J. Struct. Funct. Genomics 8*, 173–191.

(26) He, F., Saito, K., Kobayashi, N., Harada, T., Watanabe, S., Kigawa, T., Güntert, P., Ohara, O., Tanaka, A., Unzai, S., Muto, Y., and Yokoyama, S. (2009) Structural and functional characterization of the NHR1 domain of the Drosophila neuralized E3 ligase in the notch signaling pathway. *J. Mol. Biol. 393*, 478–495.

(27) Sato, M., Kubo, M., Aizawa, T., Kamo, N., Kikukawa, T., Nitta, K., and Demura, M. (2005) Role of putative anion-binding sites in cytoplasmic and extracellular channels of *Natronomonas pharaonis* Halorhodopsin. *Biochemistry 44*, 4775–4784.

(28) Hasegawa, C., Kikukawa, T., Miyauchi, S., Seki, A., Sudo, Y., Kubo, M., Demura, M., and Kamo, N. (2007) Interaction of the halobacterial transducer to a halorhodopsin mutant engineered so as to bind the transducer: Cl^- circulataion within the extracellular channel. *Photochem. Photobiol. 83*, 293–302.

(29) Chizhov, I., Engelhard, M., Chernavskii, D. S., Zubov, B., and Hess, B. (1992) Temperature and pH sensitivity of the O_{640} intermediate of the bacteriorhodopsin photocycle. *Biophys. J. 61*, 1001–1006.

(30) Tamogami, J., Kikukawa, T., Miyauchi, S., Muneyuki, E., and Kamo, N. (2009) A tin oxide transparent electrode provides the means for rapid time-resolved pH measurements: Application to photo-induced proton transfer of bacteriorhodopsin and proteorhodopsin. *Photochem. Photobiol. 85*, 578–589.

(31) Iwamoto, M., Hasegawa, C., Sudo, Y., Shimono, K., Araiso, T., and Kamo, N. (2004) Proton release and uptake of *pharaonis* phoborhodopsin (sensory rhodopsin II) reconstituted into phospholipid. *Biochemisty 43*, 3195–3203.

(32) Ren, L., Martin, C. H., Wise, K. J., Gillespie, N. B., Luecke, H., Lanyi, J. K., Spudich, J. L., and Birge, R. R. (2001) Molecular Mechanism of Spectral Tuning in Sensory Rhodopsin II. *Biochemistry 40*, 13906–13914.

(33) Tamogami, J., Kikukawa, T., Ikeda, Y., Takemura, A., Demura, M., and Kamo, N. (2010) The photochemical reaction cycle and photoinduced proton transfer of sensory rhodopsin II (phoborhodopsin) from *Halobacterium salinarum*. *Biophys. J. 98*, 1353–1363.

(34) Balashov, S. P. (2000) Protonation reactions and their coupling in bacteriorhodopsin. *Biochim. Biophys. Acta 1460*, 75–94.

(35) Luecke, H., Schobert, B., Lanyi, J. K., Spudich, E. N., and Spudich, J. L. (2001) Crystal structure of sensory rhodopsin II at 2.4 Å: Insight into color tuning and transducer interaction. *Science 293*, 1499–1503.

(36) Royant, A., Nollert, P., Edman, K., Neutze, R., Landau, E. M., Pebay-Peyroula, E., and Navarro, J. (2001) X-ray structure of sensory rhodopsin II at 2.1-Å resolution. *Proc. Natl. Acad. Sci. U.S.A. 98*, 10131–10136.

(37) Gordeliy, V. I., Labahn, J., Moukhametzianov, R., Efremov, R., Granzin, J., Schlesinger, R., Buldt, G., Savopol, T., Scheidig, A. J., Klare,

dx.doi.org/10.1021/bi2009932|*Biochemistry* 2011, 50, 8888–8898

J. P., and Engelhard, M. (2002) Molecular basis of transmembrane signalling by sensory rhodopsin II-transducer complex. *Nature 419*, 484–487.

(38) Wu, J., Ma, D., Wang, Y., Ming, M., Balashov, S. P., and Ding, J. (2009) Efficient approach to determine the pKa of the proton release complex in the photocycle of retinal proteins. *J. Phys. Chem. B 113*, 4482–4491.

(39) Brown, L. S., Dioumaev, A. K., Needleman, R., and Lanyi, J. K. (1998) Connectivity of the retinal Schiff base to Asp85 and Asp96 during the bacteriorhodopsin photocycle: The local-access model. *Biophys. J. 75*, 1445–1465.

(40) Lu, M., Balashov, S. P., Ebrey, T. G., Chen, N., Chen, Y. M., Menick, D. R., and Crouch, R. K. (2000) Evidence for the rate of the final step in the bacteriorhodopsin photocycle being controlled by the proton release group: R134H mutant. *Biochemistry 39*, 2325–2331.

dx.doi.org/10.1021/bi2009932|*Biochemistry* 2011, 50, 8888–8898

海藻カサノリ由来ロドプシンARIIの結晶構造

独立行政法人理化学研究所　生命分子システム基盤研究領域
和田　崇、染谷　友美、白水　美香子、横山　茂之

Abstract

膜タンパク質の１つで、真核単細胞生物の光駆動型プロトンポンプであるロドプシン「ARII」は、海藻のカサノリ由来のタンパク質で、生きた細胞を用いる一般的な発現方法では大量合成が非常に難しい。我々は、無細胞タンパク質合成技術※1を用いることで、ARIIの機能を保持したまま大量合成することに初めて成功し、ARIIの機能を詳細に解析することができた。また、人工脂質二重膜中での膜タンパク質の結晶化が可能な脂質メソフェーズ法※2をARIIに適用し、結晶化に成功した。そして、SPring-8のBL41XUでX線回折実験を行い、3.2 Å分解能で立体構造を決定した。これは、真核単細胞生物由来のロドプシンとして初めての構造解析例となる。

今回用いた無細胞タンパク質合成技術による膜タンパク質の合成方法は、医薬品開発など産業上有用な膜タンパク質の機能や構造の解析などに幅広く適用されることが期待される。

1. はじめに

膜タンパク質は、エネルギー生産、物質輸送、情報伝達など生命の維持に重要な役割を担うだけでなく、多くの病気に関与していることから、その構造と機能の解明により、医薬品を合理的に設計することが可能になると期待されている。タンパク質の構造と機能の解析のためには大量の試料が必要とされるが、組換え動物細胞などを用いた従来の膜タンパク質の合成方法では、その合成量が少ないうえに、合成の途中で変性しやすいなどの問題があり、大量合成が困難だった。

そこで本研究グループは、文部科学省大規模研究開発事業「ターゲットタンパク研究プログラム」で理化学研究所（理研）が開発を進めている無細胞タンパク質合成技術や脂質メソフェーズ法を用いた結晶化技術を駆使し、膜タンパク質の合成と結晶化およびその構造と機能の解析に挑んだ。

2. ロドプシンタンパク質

生命現象と光には深い関わりがあり、そこで重要な役割を果たしている物質のひとつがロドプシンである。ロドプシンはレチナール分子を含む膜タンパク質である。多くの薬剤標的となっている膜タンパク質であるGタンパク質共役受容体（GPCR）と同じ７回膜貫通構造を持ち、そのタンパク質部分（オプシン）の第７ヘリックスにあるリジン残基とレチナール分子がシッフ塩基結合してオプシンに内包されると赤～紫色を呈する。

動物の網膜に存在するロドプシンは、光を受けるとレチナール分子の立体構造変化（11-*cis*からall-*trans*への立体異性化）が起こり、Gタンパク質と相互作用してシグナル伝達を行う。また、微生物においても様々なロドプシンが発見されているが、この中で最もよく研究されているのが好塩菌*Halobacterium*由来のバクテリオロドプシン（BR）である。BRが光を受けるとレチナール分子を異性化する光サイクルが始まり、１サイクルあたり１分子のプロトンが細胞質側から細胞外側に輸送される。微生物においては、BRのようなプロトンポンプのほか、塩化物イオンを細胞質側へポンプするハ

※１無細胞タンパク質合成技術：生命体に依存しない人工的なシステムで、細胞からタンパク質合成に必要な成分一式を抽出し、これに目的のタンパク質をコードする遺伝子を合成装置が読み取れる形にして添加して、タンパク質を合成する技術。外部からさまざまな因子を加えることが容易であり、反応条件の変更や最適化も容易であるなど、多くの優れた特徴を持つ。

※２脂質メソフェーズ法：人工脂質二重膜中で膜タンパク質の結晶化を行う新しい技術。生体外で不安定な膜タンパク質の結晶化に適している。

ロロドプシン（HR）、生体が光に反応して光源方向に移動する性質（走光性）に関する情報伝達を行うセンサリーロドプシンなどが知られている。なお視物質型ロドプシンと微生物型ロドプシンではアミノ酸配列の類縁性が小さく、進化的に別の道筋をたどって今日の構造に収斂したものと考えられる。

近年、藻類の遺伝子解析から、これまでに知られていなかったオプシンが次々に発見された。2003年、緑藻クラミドモナス *Chlamydomonas* からチャネルロドプシンChR2が同定された。ChR2に光が照射されるとゲートが開き、ナトリウムなどの陽イオンが濃度勾配に従って輸送される。組換え技術でChR2を発現した神経細胞（ニューロン）に光を照射すると脱分極し、神経興奮が引き起こされた。同様にHRを発現したニューロンに光照射すると過分極が起きた。この研究分野は、オプトジェネティクス（光遺伝学）と呼ばれ、進展が目覚ましい。また2006年には、海藻カサノリ *Acetabularia acetabulum* から新規のオプシン（AR）の遺伝子が同定され、アフリカツメガエル卵母細胞内で発現させたARに、細胞内のプロトンを積極的に汲み出す活性が認められ、光駆動型プロトンポンプであることが確認された。ARの生理的な役割は今でもよくわかっていないが、カサノリの配偶子がもつ走光性と関係しているかもしれない。

3. ARIIタンパク質の合成

今回、我々はカサノリから新たな微生物型オプシン（ARII）の遺伝子を同定した[1]。そして、ARII遺伝子を導入した組換えアフリカツメガエル卵母細胞に光を照射すると電流が発生することがわかった。さらに機能解析を進めるためには、ARIIタンパク質を純度高く大量に取得する必要がある。しかし、多くの研究者がARIIを得ようと、大腸菌に遺伝子を導入してタンパク質を生産させるといった生きた細胞を用いる一般的な方法を試みていたが、発現量が非常に低く成功例が無かった。大腸菌では、膜タンパク質の多くが細胞質膜に挿入されるため、生きている細胞で大量発現させると致死的になる現象が散見される。これは膜構造が破壊されるためと推測されている。死に至らない場合でも、生き延びるために構造遺伝子やプロモーターに変異が入ることが多く、その場合は目的タンパク質の発現量が極端に少なくなる。一方、無細胞タンパク質合成技術は転写と翻訳のみを基本とした試験管内反応であるため、そのようなリスクを回避できる。そこで今回、理研で開発した膜タンパク質の無細胞タンパク質合成技術[2]を応用した。具体的には、大腸菌由来のタンパク質合成反応液に脂質と界面活性剤を加え、ARII遺伝子を組み込んだプラスミドDNAを添加して、天然の細胞膜に見立てた人工の脂質二重膜（リポソーム）中でARIIを合成した。脂質二重膜は、試験管内で実際の細胞膜と同様な構造を持っているため、活性体と呼ばれる正しい形と機能を保持した状態で膜タンパク質を得ることが可能である。ここに、ロドプシンに必須のall-*trans*型のレチナール溶液を添加して反応させたところ、反応開始前には反応液がオレンジジュースのような黄色を呈していたが、30℃で3時間保温したところ、トマトジュースのような赤色に変わり、ロドプシンの合成が進んでいることが一目瞭然であった。合成されたARIIは合成と同時に形成されたリポソーム内に移行し、反応終了後に遠心分離によって沈殿として回収することができた。この膜画分では、27 ml合成反応液あたり4.5 mgの収量で、ARII分子が脂質画分の約50％以上を占めるという大量発現が確認された。この沈殿に界面活性剤を含むバッファー溶液を添加するとARIIが可溶化し、続いてNiアフィニティカラムとゲルろ過カラムによる精製を行った。最後に限外ろ過により濃縮し45 mg/mlとした。

無細胞タンパク質合成技術によって大量合成・精製されたARIIは、複数の生化学的および物理化学的実験の結果からプロトンポンプ活性が確認された[1]。

4. ARIIの結晶構造解析

脂質メソフェーズ法による結晶化では、ARII溶液、コレステロールを含んだ脂質モノオレインをシリンジに測り取り、ふたつのシリンジの先端同士を連結してプランジャの押し引きを繰り返して混合した。つぎにガラスプレート上に穴の空いた両面粘着シートを張り付け、プレート上の穴の中に混合試料をごく少量押し出し、その上に結晶化溶液（0.1 M Tris-HCl（pH 7.5）、6% 2-methyl-2,4-pentanediol、14% polyethylene glycol 400）を滴下した。この上から別のガラスプレートを被せてサンドウィッチ状にして密閉した。このプレートを1～2週間、20℃で保温すると一辺の長さが0.1 mm程度、厚さが10 μmの薄い板状の赤紫色の結晶が成長した（図1）。

ARII結晶は環境の変化に弱く、一度ガラスプレートを剥がして、外気に触れさせると数分で退色し

た。in houseのX線解析装置では一度も反射が得られず、また一見、赤色が残る凍結結晶でもビームラインで測定すると反射点の形が乱れることがしばしばで、研究室であらかじめ良さそうな凍結結晶を選定することはできなかった。そこで何枚もの結晶化プレートをBL41XUのビームラインハッチ内に持ち込み、そこで開封してすぐに結晶をすくい取り－180℃の窒素気流で凍結させて反射チェックを行った。この作業を理想的な反射が得られるまで何度も繰り返した。結晶はX線照射によるダメージも受けやすく、直径10 μmに絞ったビームの照射位置を少しずつずらしてデータ収集する方法が効果的だった。得られたデータセットの分解能は3.2 Åで、位相決定はBR（PDB ID 1S54）をモデルに分子置換法で行った。これは、真核単細胞生物由来のロドプシンとしては初めての構造解析例となる。

5. ARIIの立体構造

ARII結晶の空間群は$P2_12_12_1$で、非対称単位中でテトラマー構造を取り、ARII 1分子あたり2分子のコレステロールが確認された。モノマー構造（図2）はBRなど微生物型ロドプシンの構造とよく類似し、7番目のヘリックス中のLys211がall-*trans*型レチナールとシッフ塩基結合していた。通常、αヘリックスでは主鎖のカルボニル基は4残基先のアミド基と水素結合するが、Lys211の前後周辺のアミノ酸残基は5残基分ずれた相手と水素結合し、結果Ala210のカルボニル基は水素結合の相手を失って

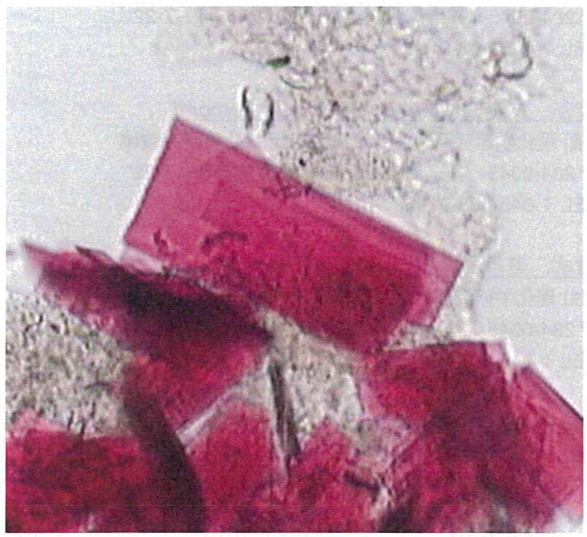

図1　脂質モノオレインのキュービック相中で成長したARII結晶

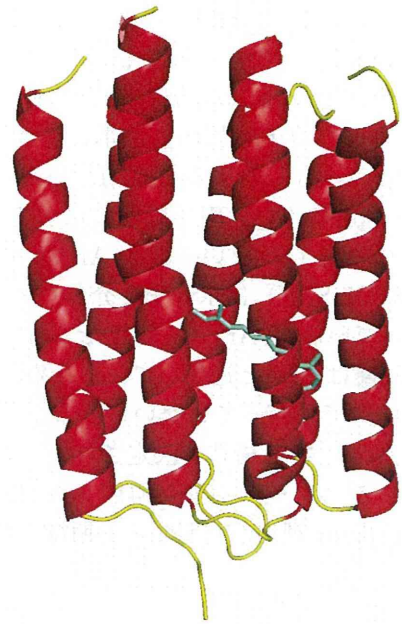

図2　ARIIのモノマー構造。ヘリックスとループを赤色と黄色で、レチナール分子を緑色で表示している。

ヘリックスが折れ、πバルジと呼ばれる構造を取っていた。この折れ曲がりはBRにも見られ特徴的である。

プロトン輸送に関するアミノ酸残基で、BRとの比較ではっきりした違いが見られるのは、Arg78（ARII）とArg82（BR）の側鎖の向きである（図3）。前者は細胞外側を向いているが、後者は細胞質側を向いている。中性付近の溶液条件では、BRはまずプロトンを細胞外に放出してから細胞質側からプロトンを取り込む（「早いプロトン放出」）。プロトン放出に先立ち、Arg82側鎖が細胞外側に反転し、Glu194（BR）とGlu194（BR）の側鎖ペアの方を向く。その結果、これらの残基のp*K*aは9.7から5.7に著しく低下し、ここからプロトンが細胞外に放出される。ふたつのGlu側鎖間には低障壁水素結合と呼ばれる特殊な水素結合が存在し、そのため容易にプロトンが放出されるとも言われる。これに対して、中性付近の溶液条件では、ARIIは先にプロトンを取りこんでから細胞外への放出を行う（「遅いプロトン放出」）。構造の観点から考察すると、Arg78（ARII）が基底状態で細胞外を向いていることや、BRのようなGlu側鎖のペアが存在しないことから、プロトンが放出されにくいのかもしれない。しかし高度好塩性アルカリ古細菌*Natronomonas*由来センサリーロドプシンII（NpSRII）のArg72側鎖も

ARIIと同様に最初から細胞外方向にあるAsp193側鎖を向いているが、中性付近でも早くプロトンを放出するため、Arg78（ARII）側鎖の向きだけでARIIの「遅いプロトン放出」が単純に説明できるわけではない。もしかするとGlu199（ARII）周辺の環境はAsp193（NpSRII）周辺に比べてより疎水性が高いのかもしれない。またArg72（NpSRII）とAsp193（NpSRII）は水分子を介したネットワークで繋がっているが、Arg78（ARII）とGlu199（ARII）の側鎖間距離は3.5 Åと近接しているため、水分子のネットワークで繋がっていないことも予想される。より高分解能のARII構造が決定されてARIIにおける水分子クラスターの実態が解明されれば、「遅いプロトン放出」の理由が判明すると期待される。

6. おわりに

今回用いた無細胞タンパク質合成技術や、脂質メソフェーズ法によって、水溶性タンパク質と比べて立体構造解析が遅れている膜タンパク質の基礎研究が大きく発展すると予想される。膜タンパク質の多くは創薬ターゲットであり、医薬品の50％以上が膜タンパク質に作用するともいわれている。膜タンパク質の詳細な立体構造解析の結果から、そこに作用する医薬品の設計が可能となるとともに、無細胞タンパク質合成技術の応用によって、膜タンパク質に対する抗体の取得が可能となることから、これらの技術は、医薬品の研究開発に大きく貢献することが期待される。

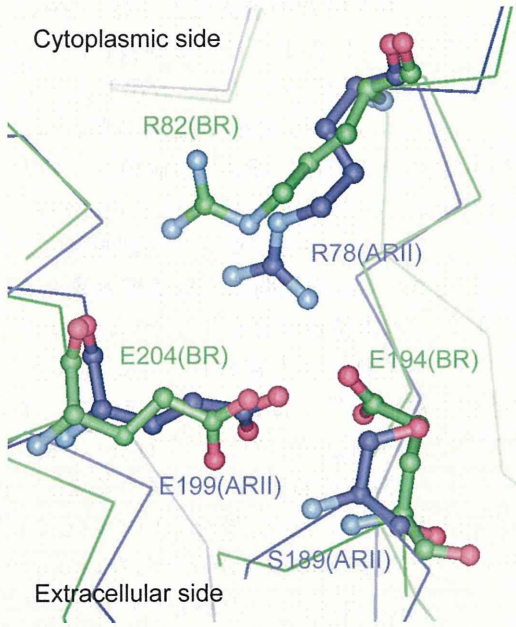

図3　プロトン放出に関与するアミノ酸残基。ARIIとBRを青色と緑色で表し、構造を重ね合わせている。

7. 謝辞

本研究は、BL41XU　2011B1005（成果公開優先利用課題）、文部科学省大規模研究開発事業「ターゲットタンパク研究プログラム」の一環として行われました。BL41XUでの測定にあたりましてご協力いただきました山本雅貴先生、河野能顕先生に厚くお礼申し上げます。また、本稿の執筆にあたりましては、共著者である下野和実先生、田母神淳先生、加茂直樹先生（松山大学）、宮内正二先生（東邦大学）、菊川峰志先生（北海道大学）、So Young Kim先生、Kwang-Hwan Jung先生（西江大学校）、新屋直子先生、羽藤正勝先生（理化学研究所　生命分子システム基盤研究領域）に厚くお礼申し上げます。

参考文献

[1] T. Wada, K. Shimono, T. Kikukawa, M. Hato, N. Shinya, S. Y. Kim, T. Kimura-Someya, M. Shirouzu, J. Tamogami, S. Miyauchi, K. H. Jung, N. Kamo and S. Yokoyama: J. Mol. Biol. **411** (2011) 986-998.

[2] K. Shimono, M. Goto, T. Kikukawa, S. Miyauchi, M. Shirouzu, N. Kamo and S. Yokoyama: Protein Sci. **18** (2009) 2160-2171.

和田　崇　WADA Takashi
(独) 理化学研究所　生命分子システム基盤研究領域
〒234-0045　神奈川県横浜市鶴見区末広町1-7-22
TEL：045-503-9196

染谷　友美　KIMURA-SOMEYA Tomomi
(独) 理化学研究所　生命分子システム基盤研究領域
〒234-0045　神奈川県横浜市鶴見区末広町1-7-22
TEL：045-503-9196

白水　美香子　SHIROUZU Mikako
(独) 理化学研究所　生命分子システム基盤研究領域
〒234-0045　神奈川県横浜市鶴見区末広町1-7-22
TEL：045-503-9196

横山　茂之　YOKOYAMA Shigeyuki
(独) 理化学研究所　生命分子システム基盤研究領域
〒234-0045　神奈川県横浜市鶴見区末広町1-7-22
TEL：045-503-9196
e-mail：yokoyama@riken.jp